Suppressing chaotic oscillations of a tether anchored to the Phobos surface under the L1 libration point

Vladimir S. Aslanov[1]

Moscow Aviation Institute (National Research University), 4, Volokolamskoe Shosse, A-80, GSP-3, Moscow, Russia

Abstract

The paper deals with the problem of the chaotic behaviour of a tethered system anchored on the Phobos surface directly under the L1 collinear libration point. Two gravitational forces of Mars and Phobos, plus a centrifugal force due to the rotation of the Mars-Phobos system, act on the tether. These forces vary with time due to the small eccentricity of the Mars-Phobos orbit. The basic assumptions are formulated in terms of a planar elliptic restricted three-body problem. The motion equations in Nechvile's variables are derived in polar coordinates relative to the anchor point of the tether. The motion of the tethered system is divided into perturbed and unperturbed when the eccentricity of the Mars-Phobos orbit is zero. The points of unstable equilibrium of the tether are found, which together with periodic perturbations associated with small eccentricity are the cause of chaotic behaviour of the tether. A tether length control law is proposed, which allows to suppress chaos by choosing the control coefficient. The Melnikov method is used to prove the chaotic nature of the tether and to find approximate the control coefficient needed to suppress the chaos. Verification of the obtained calculations is performed by means of Poincaré portraits for the basic nonlinear tether equation. The results of this study can be used for new Phobos exploration missions using an anchored tethered system and other future missions to study small planetary satellites in the Solar System.

Keywords: anchored tethered system; Phobos surface; control law; L1 collinear libration point; heteroclinic solutions; Melnikov method; Poincaré sections.

1. Introduction

New ideas and technical challenges associated with space tethered systems pose new scientific problems that have been and will be successfully implemented in future missions. Several books

[1] E-mail.address: *aslanov_vs@mail.ru*

[1-4] and hundreds of scientific articles (e.g. [5-26]) have explored the possibilities of tethered systems. Space technology based on tethered systems, which can be seen as an alternative and cheaper system to rocket systems, is one of the fastest developing technical fields.

The proposed work investigates a space tether as a classical tether anchored to the surface of Phobos. The peculiarity of the Martian satellite Phobos is that, at a distance of about 3.4 km from the surface of Phobos, there is an equilibrium position L1/L2 [27, 28], where the gravitational force of Mars and Phobos and the centrifugal force due to the rotation of the Mars-Phobos system are balanced. In addition, Phobos is always facing Mars with the same side. These two features allow to consider an end body anchored to the tether above the point L1/L2 relative to Phobos as a tether on which the above three forces act. Unlike a mathematical pendulum, there is not one gravitational force, but two gravitational forces and one centrifugal force acting on the end body (mass point). Moreover, due to the eccentricity of the orbit of the Mars-Phobos system, the distance between these large bodies (primaries) changes, and thus the gravitational and centrifugal forces change because of the irregular rotation of the Mars-Phobos system.

What is the practical use of such the anchored tethered system? There are at least three options:

- a spacecraft attached to the tether can "hover" over Phobos for any time without using jet propulsion to explore its surface;
- this tethered system can be used as a space elevator to carry the necessary equipment to the surface of Phobos and soil samples back in the opposite direction.
- realisation of a mission similar to the Martian Moons eXploration (MMX) [29, 30] for transfer to distant retrograde orbits (DROs), which are also called quasi-satellite orbits (QSOs) [61, 62], within an Earth-Mars mission.

Of course, all of these options can be combined with each other, and even combined into a single mission. A first study of this problem for the case of a circular orbit is carried out in [17].

The aim of the work is to investigate and explain a chaotic behaviour of the tether anchored to the surface of Phobos, and to design a control law to suppress the chaos. This paper only considers the tether anchored to the surface of Phobos under the L1 libration point. Everything presented in this paper can be rewritten for the case where the tether is anchored under the L2 libration point. Note also that it does not matter which pair of primaries we study, Mars-Phobos, Mars-Deimos or Earth-Moon. All results are valid for any pair of primaries.

The objective of the paper is achieved in five phases:

1. The basic assumptions are formulated in the framework of an elliptic planar restricted three-body problem, and the equations of motion in Nechvile's variables in the rotating Cartesian coordinate system are reduced to the equation of the tether in polar coordinates with respect to the anchor point located to the surface of Phobos directly under the L1 libration point.
2. The motion of the tether is classified as undisturbed, when the eccentricity of the Mars-Phobos orbit is zero, and disturbed, when the eccentricity is not zero. The stable and unstable equilibriums for the unperturbed motion are found and the perturbations caused by the small eccentricity are shown. By numerically simulating the perturbed motion, Poincaré sections are constructed which show that the small eccentricity leads to chaos.
3. A control law for the tether length is proposed based on [33], and the equation of perturbed motion of the tether is linearised by small parameters: the eccentricity of the orbit and a control parameter.
4. Approximate heteroclinic solutions are obtained in terms of hyperbolic functions, for which the Melnikov function [34] is derived. The Melnikov function gives a measure of the distance between the stable and unstable manifolds of the perturbed hyperbolic fixed points. We find an approximate value of the control parameter when the Melnikov function does not have simple zeroes and when chaos is excluded.
5. The control parameter obtained is verified by constructing Poincaré sections using the basic nonlinear equation of the perturbed tether motion.

2. Motion equations of the tether

2.1. Key assumptions

We introduce acceptable assumptions that do not distort a principled picture:

- Mars and Phobos move in elliptical orbits around a common centre of mass with a small eccentricity $(e = 0.0151)$.
- The mass m of the tethered end-point M is significantly less than the primaries' masses m_1 and m_2

$$m \ll m_2 < m_1 . \qquad (1)$$

- The tether is inextensible and massless rigid rod.
- In all considered cases, only in-plane motion is studied.

2.2. Motion equations in polar coordinates relative to the anchor point

We derive the planar motion equations of end-point of the tether M in gravitational fields of two primaries M_1 and M_2 (Mars-Phobos) in polar coordinates relative to the anchored point on the Phobos surface in terms of the restricted elliptic three-body problem [27]. The distance between the two primaries is

$$r = \frac{p}{1+e\cos f}, \tag{2}$$

where p is the semilatus rectum, e is the eccentricity of the two-body orbit of the primaries, and f is the true anomaly. In the barycentre-centred synodic coordinate system Oxy (Fig. 1), which rotates with the two primaries and using Nechvile's variables (ξ,η), the end-point motion can be described in dimensionless form as [27, 28]

$$\xi'' - 2\eta' = \frac{1}{1+e\cos f}\frac{\partial\Omega}{\partial\xi}, \tag{3}$$

$$\eta'' + 2\xi' = \frac{1}{1+e\cos f}\frac{\partial\Omega}{\partial\eta}, \tag{4}$$

where Ω is the potential function given by

$$\Omega = \frac{1}{2}\left(\xi^2+\eta^2\right) + \frac{1-\mu}{r_1} + \frac{\mu}{r_2}, \qquad \left(0<\mu\le\frac{1}{2}\right) \tag{5}$$

$$r_1 = \sqrt{(\xi+\mu)^2+\eta^2}, \qquad r_2 = \sqrt{(\xi+\mu-1)^2+\eta^2} \tag{6}$$

$$\mu = \frac{m_2}{m_1+m_2}, \qquad \nu = \frac{m_1}{m_1+m_2} = 1-\mu, \tag{7}$$

where $(.)' = \dfrac{d}{df}(.)$ and $(.)'' = \dfrac{d^2}{df^2}(.)$. The dimensionless coordinates of the tether anchor point and the tether length are entered as follows

$$\sigma = \frac{(1-\mu)p - a}{p}, \quad \lambda = \frac{l}{p}. \tag{8}$$

Here a is the distance between the anchor point A and the centre of Phobos. Position of the end-point M relative to the anchored point in a polar reference frame (l,α) is defined by substituting the variables

$$\xi=\sigma-\lambda k\cos\alpha,\ \eta=-\lambda k\sin\alpha\,, \tag{9}$$

where $k=1+e\cos f$.

Eqs. (3) and (4) in the polar reference frame are written as

$$\alpha''+\Phi_\alpha=0\,, \tag{10}$$

$$\lambda''+\Phi_\lambda=-\bar{T}\,, \tag{11}$$

where $\bar{T}$ is the dimensionless tether tension force,

$$\Phi_\alpha=-\frac{\sin\alpha}{\lambda k^2}\left(\sigma-\frac{\nu(\mu+\sigma)}{\rho_1^3}-\frac{\mu(-\nu+\sigma)}{\rho_2^3}\right)-\frac{2e}{k}(1+\alpha')\sin f+\frac{2}{\lambda}\lambda'(1+\alpha')\,, \tag{12}$$

$$\Phi_\lambda=\frac{\cos\alpha}{k^2}\left[\sigma-\frac{\nu(\mu+\sigma)}{\rho_1^3}-\frac{\mu(-\nu+\sigma)}{\rho_2^3}\right]-\frac{\lambda}{k}\left[k+\frac{-1+\mu}{\rho_1^3}-\frac{\mu}{\rho_2^3}\right]-$$

$$\lambda(2+\alpha')\alpha'-\frac{2e}{k}\lambda'\sin f\,, \tag{13}$$

where dimensionless distances between the primaries and the end-point are

$$\rho_1=\sqrt{k^2\lambda^2+(\mu+\sigma)^2-2k\lambda(\mu+\sigma)\cos\alpha}\,, \tag{14}$$

$$\rho_2=\sqrt{k^2\lambda^2+(-\nu+\sigma)^2-2k\lambda(-\nu+\sigma)\cos\alpha}\,. \tag{15}$$

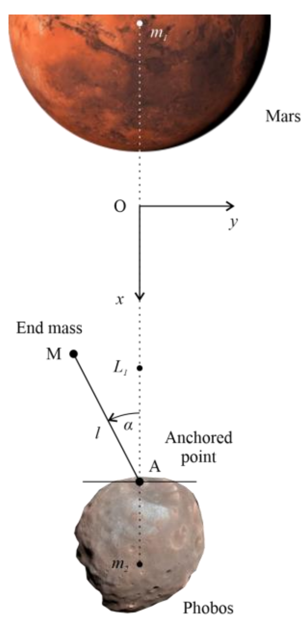

Fig. 1. The frame Oxy and the polar frame (l,α).

2.2. A tether of constant length. Perturbed and unperturbed motion

Assuming that a tether length is constant

$$l = const \to \lambda' = 0,\ \lambda'' = 0 \tag{16}$$

In this case, Eq. (10) is rewritten as follows

$$\alpha'' + \Phi_\alpha = 0\,, \tag{17}$$

where

$$\Phi_\alpha = -\frac{\sin\alpha}{\lambda(1+e\cos f)^2}\left(\sigma + \frac{(-1+\mu)(\mu+\sigma)}{\rho_1^3} - \frac{\mu(-1+\mu+\sigma)}{\rho_2^3}\right) - \frac{2e}{1+e\cos f}(1+\alpha')\sin f\ . \tag{18}$$

In the case of an unperturbed motion, where the primaries move on circular orbits ($e=0$) relative to its center of mass and the distance between them does not change, Eq. (18) has the form

$$\ddot{\alpha} + \Phi_{0\alpha} = 0\,, \tag{19}$$

where

$$\Phi_{0\alpha} = \Phi_\alpha\big|_{e=0} = -\frac{\sin\alpha}{\lambda}\left[\sigma + \frac{(-1+\mu)(\mu+\sigma)}{\rho_1^3} - \frac{\mu(-1+\mu+\sigma)}{\rho_2^3}\right]. \tag{20}$$

Now here

$$\rho_1 = \sqrt{\lambda^2 + (\mu+\sigma)^2 - 2\lambda(\mu+\sigma)\cos\alpha}\,, \tag{21}$$

$$\rho_2 = \sqrt{\lambda^2 + (-\nu+\sigma)^2 - 2\lambda(-\nu+\sigma)\cos\alpha}\ . \tag{22}$$

Eq. (19) has the following energy integral

$$\frac{\alpha'^2}{2} + U(\alpha) = E = const\,, \tag{23}$$

where E is the total energy, the potential energy is

$$U(\alpha) = \int \Phi_{0\alpha}(\alpha)\,d\alpha = \frac{1}{\lambda}\left(\sigma\cos\alpha - \frac{\nu}{\lambda\rho_1} - \frac{\mu}{\lambda\rho_2}\right). \tag{24}$$

3. Unstable equilibrium, disturbances and chaos

3.1. Preliminary observations

Collinear libration points, including the L1 libration point are defined as the roots of Eq. (3) for $\xi'' = 0$, $\eta = 0$, $\eta' = 0$, $e = 0$.

For the Mars-Phobos system $\xi_{L_1} = 0.998229$.

The planar cross-section of Phobos can be considered as an ellipse if the Stickney crater is disregarded [35]. Analytically, the equation of a standard ellipse centered at the origin with a semi-major ($2a$) and a semi-minor ($2b$) axes is

$$\frac{(X - r_h)^2}{a^2} + \frac{Y^2}{b^2} = 1, \tag{25}$$

where $a = 13.0\,km$ and $b = 11.2\,km$ are the semi-major and the semi-minor axes, $r_h = 16.812\,km$ is the distance between the L1 libration point and the center of this ellipse. Then, using Eq. (8), obtain

$$\sigma = 0.998588,\ \lambda_{L_1} = \sigma - \xi_{L_1} = 0.000360. \tag{26}$$

In this case, the length of the tether is equal to

$$l_{L_1} = \lambda_{L_1} p = 3411.878\,m. \tag{27}$$

3.2 Phase portrait and bifurcation diagram

The phase portrait of the system (19) are plotted for the tether length

$$l = 4000\,m. \tag{28}$$

Fig. 2 shows the potential energy (24) and the phase portraits determined by Eq. (23). Solving the equation

$$\Phi_{0\alpha}(\alpha) = 0. \tag{29}$$

on the interval $[-2\pi, 2\pi]$ one obtains the five stable equilibrium positions

$$\alpha_s = (-2\pi,\ -\pi,\ 0,\ \pi,\ 2\pi) \tag{30}$$

and the four unstable equilibrium positions (Fig. 2)

$$\alpha_{us} = (-2\pi + 0.981,\ -0.981,\ 0.981,\ 2\pi - 0.981)\,rad. \tag{31}$$

a

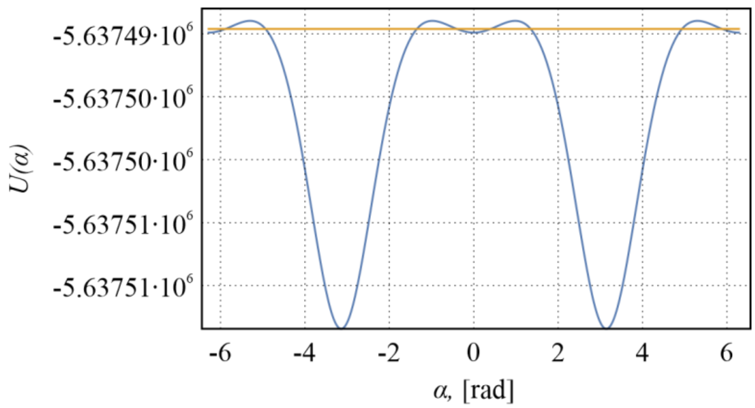

b

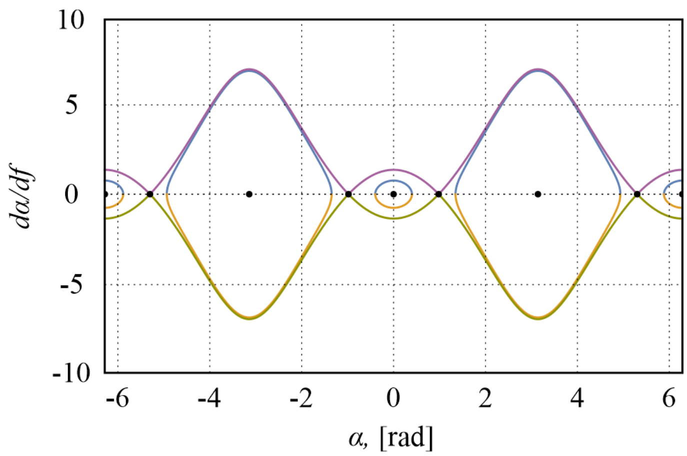

Fig. 2. (**a**) The function $U(\alpha)$ and (**b**) the phase portrait $\frac{d\alpha}{df}(\alpha)$ for the tether length $l = 4000\,m$.

As shown in Fig. 2, the phase portrait is symmetric with respect to the ordinate axis for the anchored tether without the transverse displacement. A bifurcation diagram as a function of the tether length in Fig. 3, where the solid lines correspond to unstable equilibrium positions, and dashed lines indicate stable positions in the interval $\alpha \in \left[-\frac{\pi}{2}, \frac{\pi}{2}\right]$.

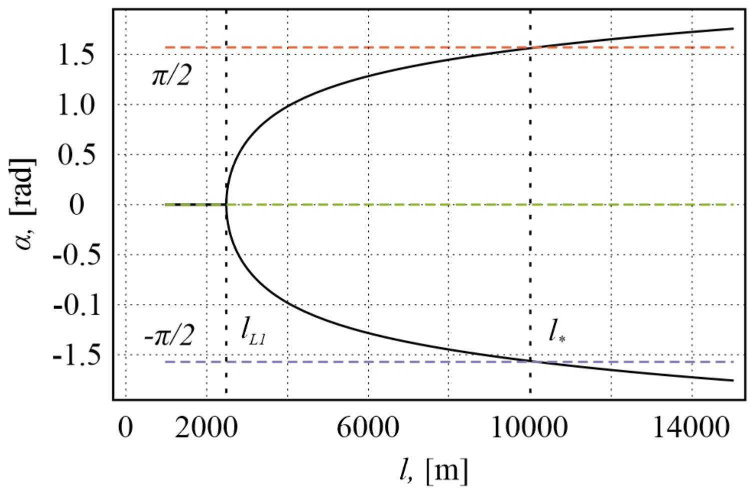

Fig. 3. Bifurcation diagram ($l_* = \lambda_* p = 10300\,m$, $l_{L_1} = \lambda_{L_1} p = 3411.878\,m$).

Obviously, for the planar model of Phobos (25), the tether deflection angle should be in the interval:

$$\alpha \in (-\frac{\pi}{2}, \frac{\pi}{2}). \tag{32}$$

The tether will touch the surface of Phobos near the attachment point if the condition (32) is violated. It is therefore clear that the tether length is also limited by the value of $l_* = \lambda_* p = 10300\,m$. On the other hand, the tether must be greater than the distance from the anchor point to the L1 libration point $l_{L_1} = \lambda_{L_1} p = 3412\,m$, otherwise the tether will not be able to hover above the surface of Phobos. For this reason, there are also the following limits for the relative length of the tether

$$\lambda \in (\lambda_{L_1}, \lambda_*), \tag{33}$$

where $\lambda_{L_1} = 0.00036$, $\lambda_* = 0.00109$.

3.3 Detecting chaos

Two circumstances determine the possibility of the occurrence of chaos: firstly, the presence of unstable equilibrium positions of the unperturbed system (19), as shown in Fig. 2, and secondly, periodic perturbations caused by the small eccentricity of the Mars-Phobos orbit. The presence of this perturbation is illustrated by the last summand in Eq. (18):

$$\frac{2e}{1+e\cos f}(1+\alpha')\sin f\ . \tag{34}$$

To study the influences of the small disturbances on the dynamics, the perturbed motion is analyzed by constructing Poincaré surfaces in the two-dimensional space (α, α'). Constructions of the Poincaré surfaces are based on the numerical integration of Eq. (17). All the trajectories shown in Figs. 4 and 5 start on the abscissa axis

$$\alpha_0 \in \left(\alpha_{us} - 0.01, \alpha_{us} + 0.01\right), \alpha_0' = 0\,. \tag{35}$$

As shown in Fig. 4, at $e = 0$ the unperturbed motion is realised and a regular phase space structure is observed, the trajectories have no intersections and the Poincaré sections coincide with the unperturbed phase portrait.

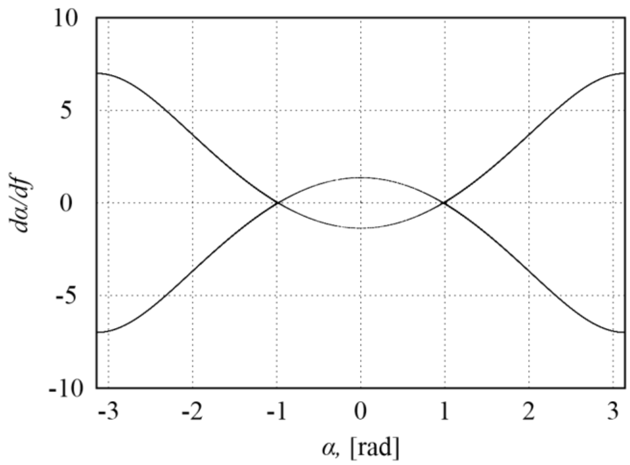

Fig. 4. Poincaré sections for $e = 0$.

The perturbations result in the complication of phase space and the occurrence of a chaotic layer near the unperturbed separatrixes as illustrated in Fig. 5.

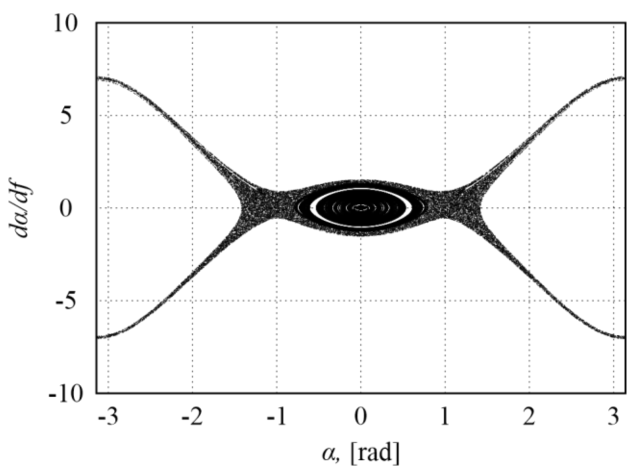

Fig. 5. Poincaré sections for $e = 0.0151$.

4. Melnikov method. Chaos suppression

4.1. The tether length control

The periodic changes in the gravitational and centrifugal forces associated with the small eccentricity of Mars-Phobos orbits lead to chaos. If, as in our case, the tether is fixed at one end, its angular motion can only be affected by changing its length. The control law of the tether, which reduces an oscillation amplitude of a classical tether, can be used in the form of [33]

$$\lambda = \lambda_0 + a\alpha' \sin\alpha \,, \tag{36}$$

where a is a small dimensionless control parameter, $\lambda_0 = const$ is the relative length of the tether at the tether equilibrium position $\alpha = 0$. The control law (36) is substituted in the basic equation of motion (10) and then this equation is expanded in a power series of small parameters a and e. Further, keeping only the first order terms, the obtained equation is written as

$$\alpha'' + F = e F_e + aF_a \,, \tag{37}$$

$$F(\alpha) = -\frac{\sin\alpha}{\lambda_0}\left[\sigma + \frac{\nu(\sigma+\mu)}{\rho_1^{\,3}} + \frac{\mu(\sigma-\nu)}{\rho_2^{\,3}}\right] +$$

$$e\frac{\sin\alpha\cos\alpha}{\lambda_0}\left[2\sigma - \frac{\nu(\sigma+\mu)\left(5\lambda_0^{\,2} + 2(\sigma+\mu)^2 - 7\lambda_0(\sigma+\mu)\cos\alpha\right)}{\rho_1^{\,5}} -\right.$$

$$\left.\frac{\mu(\sigma-\nu)\left(5\lambda_0^{\,2} + 2(\sigma-\nu)^2 - 7\lambda_0(\sigma-\nu)\cos\alpha\right)}{\rho_2^{\,5}}\right], \tag{38}$$

$$F_e(f,\alpha') = 2(1+\alpha')\sin f \tag{39}$$

$$F_a(\alpha,\alpha') = -\frac{\sin^2\alpha}{\lambda_0^{\,2}}\left[2(1+\alpha')(\sigma - \frac{\nu(\sigma+\mu)}{\rho_1^{\,3}} - \frac{\mu(\sigma-\nu)}{\rho_2^{\,3}}) + \right.$$

$$\alpha'\left(2\sigma - \frac{\nu(\sigma+\mu)\left(4\lambda_0^{\,2} + (\sigma+\mu)^2 - 5\lambda_0(\sigma+\mu)\cos\alpha\right)}{\rho_1^{\,5}} -\right.$$

$$\left.\left.\frac{\mu(\sigma-\nu)(4\lambda_0^{\,2} + (\sigma-\nu)^2 - 5\lambda_0(\sigma-\nu)\cos\alpha}{\rho_2^{\,5}}\right)\right] + \frac{2}{\lambda_0}\alpha'^2(1+\alpha')\cos\alpha \,. \tag{40}$$

Now here

$$\rho_1 = \sqrt{\lambda_0{}^2 + (\mu+\sigma)^2 - 2\lambda_0(\mu+\sigma)\cos\alpha}\,, \tag{41}$$

$$\rho_2 = \sqrt{\lambda_0{}^2 + (\sigma-\nu)^2 - 2\lambda_0(\sigma-\nu)\cos\alpha}\,, \tag{42}$$

Note that the function (38) depends only on the angle of deflection of the tether α. The disturbing torque (39) is a periodic function of the true anomaly f and the damping torque is determined by the function (40).

4.2. Melnikov method

The existence of heteroclinic intersections can be proved using the Melnikov method [34]. The perturbed second-order equation (37) is represented as two first-order differential equations

$$\alpha' = \omega = f_1 + g_1 \tag{43}$$

$$\omega' = f_2 + g_2\,, \tag{44}$$

where

$$f_1 = \omega\,, \qquad g_1 = 0\,,$$

$$f_2 = F(\alpha)\,, \qquad g_2 = eF_e(f,\alpha') + aF_a(\alpha,\alpha')\,.$$

The Melnikov function [64] for Eqs. (43) and (44) is given by

$$M^{\pm}(f_0) = \int_{-\infty}^{\infty}\{f_1[q_{\pm}^0(f)]\; g_2[q_{\pm}^0(f), f+f_0] - f_2[q_{\pm}^0(f)]\; g_1[q_{\pm}^0(f), f+f_0]\}df$$

$$= \int_{-\infty}^{\infty}\{f_1[q_{\pm}^0(f)]\; g_2[q_{\pm}^0(f), f+f_0]\}df\,, \tag{45}$$

where $q_{\pm}^0(f) = [\alpha_{\pm}(f), \omega_{\pm}(f)]$ are the solutions of the unperturbed heteroclinic orbits that are to be found.

4.3 Approximate heteroclinic solutions

To construct the Melnikov function, it is necessary to find an analytical solution explicitly for the equation of undisturbed motion on the upper and lower separatrices bounding the area centred on point $\alpha = 0$ (Fig. 2 b). The equations of unperturbed motion are obtained from Eq. (37) if the right-hand part of the equation is set equal to zero, as follows

$$\alpha'' + F(\alpha) = 0\,. \tag{46}$$

This equation has the following energy integral

$$\frac{\alpha'^2}{2}+U(\alpha)=E=const\,, \tag{47}$$

where E is the total energy, the potential energy is

$$U(\alpha)=\int F(\alpha)\,d\alpha\,. \tag{48}$$

As can be seen from Eqs. (46)-(48) and (38), Eq. (46) integrates in quadrature, but it is not possible to find its analytical solutions. We obtain an approximate solution. The nonlinear function $F(\alpha)$ is represented as a third-order power series

$$\alpha''+a_1\alpha+a_3\alpha^3=0\,, \tag{49}$$

where

$$\begin{aligned}a_1=&\frac{1}{\lambda}\left[-\sigma+\frac{\nu(\mu+\sigma)}{(-\lambda+\mu+\sigma)^3}+\frac{\mu(\sigma-\nu)}{(\lambda+\nu-\sigma)^3}\right]+\\&\frac{e}{\lambda}\left[2\sigma-\frac{\nu(\mu+\sigma)\left(-5\lambda+2(\mu+\sigma)\right)}{(-\lambda+\mu+\sigma)^4}-\frac{\mu(5\lambda+2\nu-2\sigma)(\sigma-\nu)}{(\lambda+\nu-\sigma)^4}\right],\end{aligned} \tag{50}$$

$$\begin{aligned}a_3=&\frac{1}{6}\left[\frac{\sigma}{\lambda}-\frac{\nu(\mu+\sigma)}{\lambda(-\lambda+\mu+\sigma)^3}-\frac{9\nu(\mu+\sigma)^2}{(-\lambda+\mu+\sigma)^5}-\frac{\mu(\sigma-\nu)}{\lambda(\lambda+\nu-\sigma)^3}-\frac{9\mu(\sigma-\nu)^2}{(\lambda+\nu-\sigma)^5}\right]+\\&\frac{e}{6}\left[\frac{9\nu(\mu+\sigma)^2(-6\lambda+\mu+\sigma)}{(-\lambda+\mu+\sigma)^6}+\frac{9\mu(\sigma-\nu)^2(6\lambda+\nu-\sigma)}{(\lambda+\nu-\sigma)^6}-\right.\\&\left.\frac{4}{\lambda}\left(2\sigma-\frac{\nu(\mu+\sigma)\left(-5\lambda+2(\mu+\sigma)\right)}{(-\lambda+\mu+\sigma)^4}-\frac{\mu(5\lambda+2\nu-2\sigma)(\sigma-\nu)}{(\lambda+\nu-\sigma)^4}\right)\right].\end{aligned} \tag{51}$$

This equation has the following energy integral

$$\frac{\alpha'^2}{2}+U_0(\alpha)=E=const\,. \tag{52}$$

where E is the total energy, the potential energy is

$$U_0(\alpha)=\frac{a_1}{2}\alpha^2+\frac{a_3}{4}\alpha^4\,. \tag{53}$$

Separating the variables in the energy integral (52) gives the following quadrature

$$f-f_0=\int_{\alpha_0}^{\alpha}\frac{d\alpha}{\sqrt{2(E-\frac{a_1}{2}\alpha^2-\frac{a_3}{4}\alpha^4)}}\,, \tag{54}$$

This elliptic integral can be represented as follows

$$f - f_0 = \int_{\alpha_0}^{\alpha} \frac{d\alpha}{\sqrt{-2a_3}\sqrt{(\alpha-\alpha_1)(\alpha-\alpha_2)(\alpha-\alpha_3)(\alpha-\alpha_4)}} \ . \tag{55}$$

On the separatrices the following equalities take place

$$\alpha_1 = \alpha_2 = \alpha_{us} \quad \alpha_3 = \alpha_4 = -\alpha_{us} , \tag{56}$$

then the integral (55) can be rewritten as

$$\varsigma(f - f_0) = \pm\int_{\alpha_0}^{\alpha} \frac{d\alpha}{(\alpha^2 - \alpha_{us}{}^2)} \ , \tag{57}$$

where $\varsigma = \sqrt{-2a_3}$.

The integral (57) can be easily calculated

$$\varsigma(f - f_0) = \ln\left|\frac{\alpha_{us}+\alpha}{\alpha_{us}-\alpha}\right|\Bigg|_{\alpha_0}^{\alpha} \ . \tag{58}$$

Finally, the formula (58) can be written using hyperbolic functions as

$$\alpha_+(f - f_0) = \alpha_{us}\tanh[\frac{\varsigma(f-f_0)}{2}], \qquad \omega_+(f) = (\dot{\alpha}) = \frac{1}{2} = \alpha_{us}\varsigma\,\mathrm{sech}[\frac{\varsigma(f-f_0)}{2}]^2 , \tag{59}$$

$$[\alpha_-(f - f_0), \omega_-(f - f_0)] = [-\alpha_+(f - f_0), -\omega_+(f - f_0)] . \tag{60}$$

4.4. Melnikov function

The Melnikov function (45) is rewritten taking into account equations (39) and (40)

$$M^{\pm}(f_0) = e\left(I_C^{\pm}\sin f_0 + I_S^{\pm}\cos f_0\right) + aI_A^{\pm} , \tag{61}$$

where

$$I_C^{\pm} = 2\int_{-\infty}^{\infty}\omega_{\pm}\left(1+\omega_{\pm}\right)\cos f df \ . \tag{62}$$

$$I_S^{\pm} = 2\int_{-\infty}^{\infty}\omega_{\pm}\left(1+\omega_{\pm}\right)\sin f df \ , \tag{63}$$

$$I_C^{\pm} = -\frac{1}{\lambda_0{}^2}\int_{-\infty}^{\infty}\omega_{\pm}\Bigg\{\sin^2\alpha_{\pm}\Bigg[2(1+\omega_{\pm})(\sigma - \frac{\nu(\sigma+\mu)}{\rho_1{}^3} - \frac{\mu(\sigma-\nu)}{\rho_2{}^3}) +$$

$$\omega_{\pm}\Bigg(2\sigma - \frac{\nu(\sigma+\mu)\left(4\lambda_0{}^2 + (\sigma+\mu)^2 - 5\lambda_0(\sigma+\mu)\cos\alpha_{\pm}\right)}{\rho_1{}^5} -$$

$$\frac{\mu(\sigma-\nu)(4\lambda_0^{\ 2}+(\sigma-\nu)^2-5\lambda_0(\sigma-\nu)\cos\alpha_\pm)}{\rho_2^{\ 5}}\Bigg)\Bigg]+$$

$$2\lambda_0\omega_\pm^{\ 2}(1+\omega_\pm)\cos\alpha_\pm\Big\}df\ , \tag{64}$$

Here

$$\rho_1=\sqrt{\lambda_0^{\ 2}+(\mu+\sigma)^2-2\lambda_0(\mu+\sigma)\cos\alpha_\pm}\ , \tag{65}$$

$$\rho_2=\sqrt{\lambda_0^{\ 2}+(\sigma-\nu)^2-2\lambda_0(\sigma-\nu)\cos\alpha_\pm}\ . \tag{66}$$

The Melnikov function give us a measure of the distance between the stable and unstable manifolds of the perturbed hyperbolic fixed points. Thus, if $M^\pm(f_0)=0$ there are transverse intersections between the stable and unstable trajectories. From formula (61), that the Melnikov function has no simple zeros if the following condition is satisfied

$$a^\pm>\frac{\sqrt{\left(I_C^\pm\right)^2+\left(I_S^\pm\right)^2}}{\left|I_A^\pm\right|}=a_*^\pm\ . \tag{67}$$

At a tether length of 4000 m for the upper and lower separatrix, the critical value of the control coefficient, respectively, is equal to

$$a_*^+=0.545\times10^{-5}. \tag{68}$$

$$a_*^-=0.461\times10^{-6}. \tag{69}$$

Fig. 6 depicts the Melnikov function for different values of the control parameter a .

a

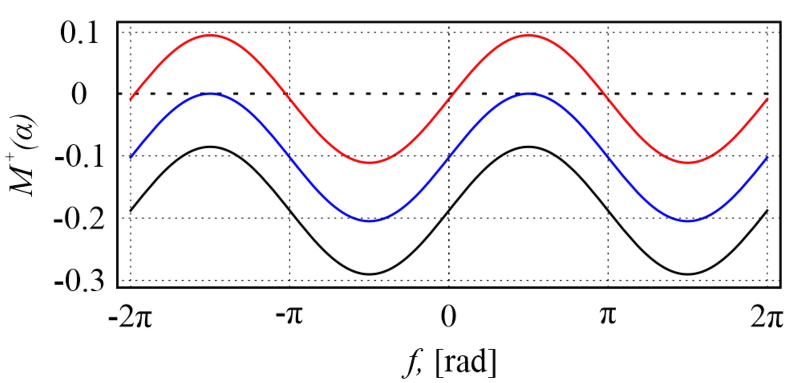

b

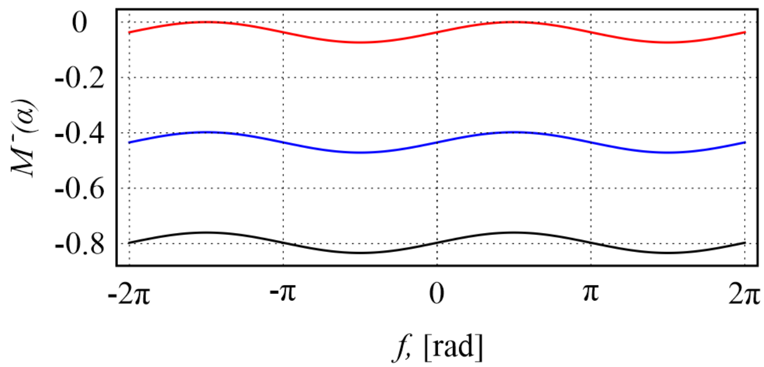

Fig. 6. (**a**)The Melnikov function for the upper separatrix $M^{+}(f_0)$ and (**b**) for the lower separatrix $M^{-}(f_0)$ in the tether length $l = 4000\,m$ ($a = a_*^- = 4.614\times10^{-7}$ - red, $a = a_*^+ = 5.452\times10^{-6}$ - blue, $a = 10^{-5}$ - black).

Note that without control of the tether length ($a = 0$) the Melnikov function

$$M^{\pm}(f_0) = e\left(I_c^{\pm}\sin f_0 + I_s^{\pm}\cos f_0\right), \tag{70}$$

has simple zeros. We observe chaos as shown in Fig. 5.

5. Poincaré sections

The Melnikov functions are obtained for the linearised tether equation (37) by means of approximate heteroclinic solutions (59) and (60). The verification of the control coefficient is done by numerical integration of the basic tether equation (17) and the construction of Poincaré portraits. Figs. 7-9 show them for the following values of the control variable:

$a = a_*^- = 0.461\times10^{-6}$ (red), $a = a_*^+ = 0.545\times10^{-5}$ (blue), $a = 10^{-5}$ (black)

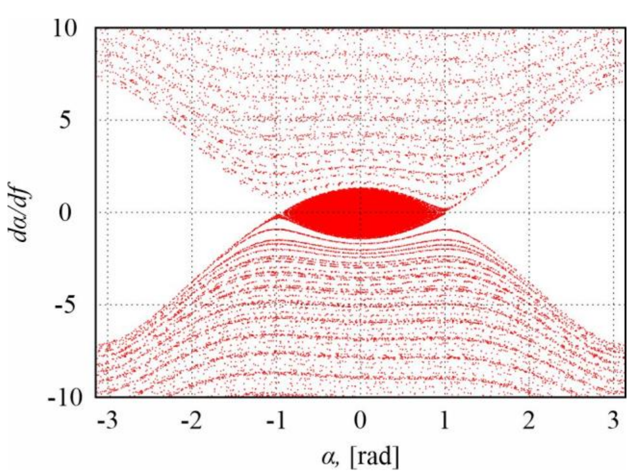

Fig. 7. Poincaré sections for $a = a_*^- = 4.614\times10^{-7}$

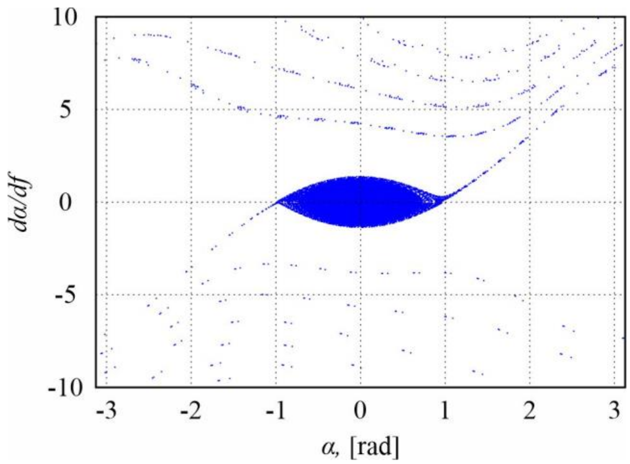

Fig. 8. Poincaré sections for $a = a_*^+ = 5.452 \times 10^{-6}$

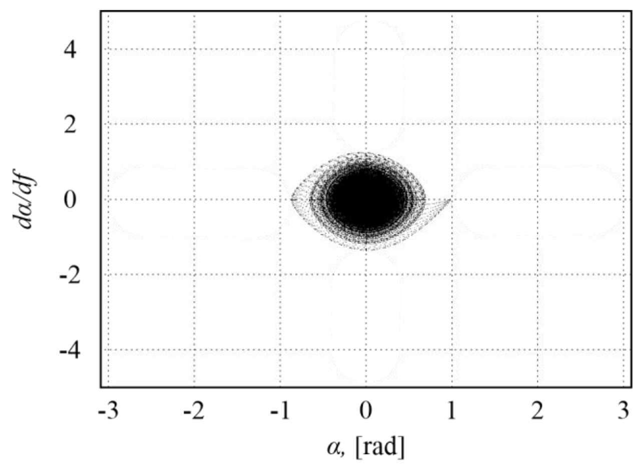

Fig. 9. Poincaré sections for $a = 10^{-5}$

Figs. 7-9 show the effectiveness of the control law (36) to suppress chaos of the tether. For the tether length of 4000 m, this occurs at $a = 10^{-5}$. This value is almost 2 times higher than the value obtained by the Melnikov method (68). This is due to the approximations that have been made when using the Melnikov method. Note that the control coefficient a is very small, of the order of 10^{-5}, in both cases.

The question of how the tether length changes when the control law (36) is implemented to suppress the chaotic behaviour of the tether has not been investigated. From Fig. 10 it can be seen that for the following values of the control parameter and the initial length of the tether

$$a = 10^{-5}, \; l_0 = 4000\, m \tag{71}$$

the tether length changes relative to the initial value with an amplitude of 1.5m and a periodicity of half the orbital period of Mars-Phobos.

a

b

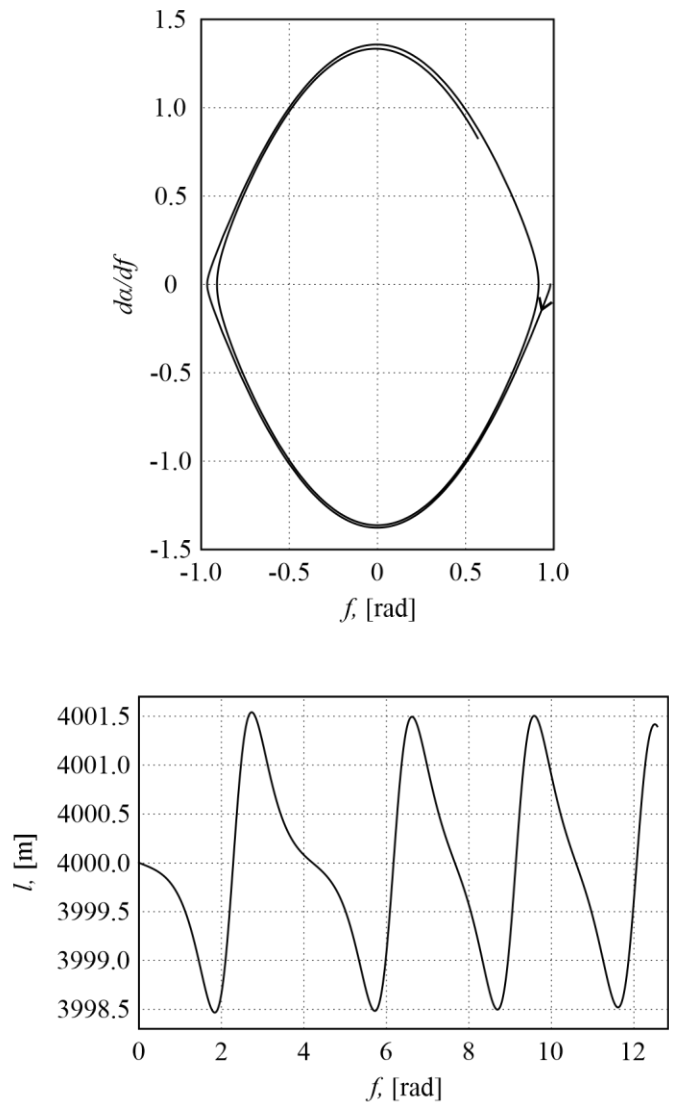

Fig. 10. (**a**) The phase portrait $\frac{d\alpha}{df}(\alpha)$ and (**b**) the tether length history of true anomaly for the control parameter $a = 10^{-5}$ and the initial length of the tether $l_0 = 4000\,m$

6. Conclusions

In the framework of the restricted elliptic three-body problem, a tether anchored on a surface directly under the L1 collinear libration point is considered. The main findings of the paper can be summarized in the following way:

1. Chaos in the behavior of the anchored tether due to the small eccentricity of the Mars-Phobos orbit is detected.

2. The existence of the chaotic behavior of the anchored tether is proved analytically by means of Melnikov method.
3. The tether length control law for chaos suppression is proposed.
4. By plotting Poincaré maps using the basic nonlinear tether equation, the effectiveness of the tether control law is verified.

Declaration of Competing Interest

The author declare that he has no known competing financial interests or personal relationships that could have appeared to influence the work reported in this paper.

References

[1] Beletsky V.V., Levin E.M. Dynamics of space tether systems. Univelt Incorporated, San Diego, 1993.
[2] Levin E.M. Dynamic Analysis of Space Tether Missions. Univelt Incorporated, San Diego, 2007.
[3] Troger H., Alpatov A.P., Beletsky V.V., Dranovskii V.I., Khoroshilov S.V., Pirozhenko A.V., Zakrzhevskii A.E. Dynamics of Tethered Space Systems. CRC Press, New York, 2010.
[4] Aslanov V.S., Ledkov A.S. Dynamics of Tethered Satellite Systems. Woodhead Publishing, Cambridge, 2012.
[5] Williams P., Hyslop A., Stelzer M., Kruijff M. YES2 Optimal Trajectories in Presence of Eccentricity and Aerodynamic Drag. Acta Astronautica, 64(7) (2009) 745–769. https://doi.org/10.1016/j.actaastro.2008.11.007.
[6] Williams P., Blanksby C., Trivailo P. Tethered Planetary Capture Maneuvers. Journal of Spacecraft and Rockets, 41(4) (2004) 603–613. https://doi.org/10.2514/1.1024.
[7] Jung W., Mazzoleni A., Chung J. Nonlinear dynamic analysis of a three-body tethered satellite system with deployment/retrieval. Nonlinear Dyn. 82 (2015) 1127–1144. https://doi.org/10.1007/s11071-015-2221-z.

[8] Huang P., Zhang F., Chen L., Meng Z., Zhang Y., Liu Z., Hu Y. A review of space tether in new applications. Nonlinear Dyn. 94 (2018) 1–19. https://doi.org/10.1007/s11071-018-4389-5.
[9] Yu B., Xu S., Jin D. Chaos in a tethered satellite system induced by atmospheric drag and Earth's oblateness. Nonlinear Dyn. 101 (2020) 1233–1244. https://doi.org/10.1007/s11071-020-05844-8.
[10] Shi G., Zhu Z., Orbital radius keeping of floating partial space elevator in cargo transposition. Astrodyn. 7, (2023) 259–269. https://doi.org/10.1007/s42064-022-0156-y.
[11] Kumar K.D., Kumar K. Attitude Maneuver of Dual Tethered Satellite Platforms Through Tether Offset Change. Journal of Spacecraft and Rockets, 38, 2 (2001) 237–242. https://doi.org/10.2514/2.3676.
[12] Kumar K., Yasaka T. Rotation formation flying of three satellites using tethers. Journal of Spacecraft and Rockets. 41(6) (2004) 973–85. https://doi.org/10.2514/1.14251.
[13] Cartmell M., McKenzie D., A review of space tether research. Prog. Aerosp. Sci. 44(1) (2008) 1–21. https://doi.org/10.1016/j.paerosci.2007.08.002.
[14] Mashayekhi M., Misra A. Optimization of tether-assisted asteroid deflection. Journal of Guidance, Control, and Dynamics, 37(3) (2014) 898-906. https://doi.org/10.2514/1.60176.
[15] Kempton K., Pearson J., Levin E., Carroll J., Amzajerdian F. Phase 1 Study for the Phobos L1 Operational Tether Experiment (PHLOTE), End Report, NASA (2018) 1-91. https://ntrs.nasa.gov/search.jsp?R=20190000916.
[16] Sun G., Zhu Z. Fractional-order tension control law for deployment of space tether system. Journal of Guidance, Control, and Dynamics. 37(6) (2014) 2057–167. https://doi.org/10.2514/1.G000496.
[17] Aslanov V. Prospects of a tether system deployed at the L1 libration point. Nonlinear Dyn. 106 (2021) 2021–2033. https://doi.org/10.1007/s11071-021-06884-4.
[18] Aslanov V. Dynamics of a Phobos-anchored tether near the L1 libration point. Nonlinear Dyn. 111 (2023) 1269–1283. https://doi.org/10.1007/s11071-022-07892-8.
[19] Aslanov V. Tether System in Martian-Moons-eXploration-Like Mission for Phobos Surface Exploration. Journal of Spacecraft and Rockets. (2023) 1-8. https://doi.org/10.2514/1.A35777.
[20] Aslanov V., Ledkov A. Survey of Tether System Technology for Space Debris Removal Missions. Journal of Spacecraft and Rockets. 1 (2023) 81. https://doi.org/10.2514/1.A35646.
[21] Aslanov V. Swing principle for deployment of a tether-assisted return mission of a re-entry capsule. Acta Astronautica. 120 (2016) 154-158. http://dx.doi.org/10.1016/j.actaastro.2015.12.020.

[22] Aslanov V. A double pendulum fixed at the L1 libration point: a precursor to a Mars–Phobos space elevator. Nonlinear Dyn. 112 (2024) 775–791. https://doi.org/10.1007/s11071-023-09108-z.

[23] Misra A., Amier Z., Modi V. Attitude dynamics of three-body tethered systems. Acta Astronautica 17(10) (1988). 1059–1068. https://doi.org/10.1016/0094-5765(88)90189-0.

[24] Kumar K., Kumar R., Misra A. Effects of deployment rates and librations on tethered payload raising. J. Guid. Control Dyn. 15(5) (1992) 1230–1235. https://doi.org/10.2514/3.20973.

[25] Woo P., Misra A. Dynamics of a partial space elevator with multiple climbers. Acta Astronautica 67(7–8) (2010) 753–763. https://doi.org/10.1016/j.actaastro.2010.04.023.

[26] Shi G., Zhu Z., Zhu Z. H. Libration suppression of tethered space system with a moving climber in circular orbit. Nonlinear Dyn. 91 (2018) 923–937. https://doi.org/10.1007/s11071-017-3919-x.

[27] Szebehely V. The Restricted Problem of Three Bodies, Academic Press Inc., New York, 1967.

[28] Markeev A.P. Libration Points in Celestial Mechanics and Astrodynamics, Nauka, Moscow [in Russian], 1978.

[29] Kawakatsu Y., Kuramoto K., Usui T., et al. Imada, Preliminary Design of Martian Moons eXploration (MMX). Acta Astronautica, 202 (2023) pp. 715–728. https://doi.org/10.1016/j.actaastro.2022.09.009.

[30] Baresi N., Dei Tos D., Ikeda H., Kawakatsu Y. Trajectory Design and Maintenance of the Martian Moons eXploration Mission Around Phobos. Journal of Guidance, Control, and Dynamics. 44 (5) (2021) 996–1007. https://doi.org/10.2514/1.G005041.

[31] Kogan A. Distant satellite orbits in the restricted circular three-body problem. Cosmic Research 24 (1989) 705-710.

[32] Sidorenko V., Neishtadt A., Artemyev A., Zelenyi L. Quasi-satellite orbits in the general context of dynamics in the 1:1 mean motion resonance: perturbative treatment. Celest Mech Dyn Astr. 120 (2014) 131–162. https://doi.org/10.1007/s10569-014-9565-4.

[33] Aslanov V. Stability of a pendulum with a moving mass: the averaging method. Journal of Sound and Vibration, 445 (2019) 261-269. https://doi.org/10.1016/j.jsv.2019.01.021.

[34] Melnikov V. On the stability of the center for time periodic perturbations. Trans. Moscow Math. Soc. 12 (1963) 1–56.

[35] Lucchetti A., Cremonese G., Pajola M., et al. New simulation of Phobos Stickney crater. (2015) URL: http://hdl.handle.net/20.500.12386/26076.